of the spectra of various $Fe^{II}TMP$ low-spin derivatives will be published elsewhere.[47]

Concluding Remarks

The major monomeric species in water and their spin states as deduced from the present study and in consideration of previously reported works are shown in Scheme I. Three ferric and two ferrous species are sufficient to explain the results between pH 1 and 14. Proton equilibria exist between the three ferriporphyrin species with pK_a values of ca. 5.7 and 12.3. A proton equilibrium also exists between the ferroporphyrin species with a pK_a value ca. 11.2. Although both $Fe^{III}TMP$ species in regions of pH 1–4 ($Fe^{III}TMP(H_2O)$) and pH 8–11 ($Fe^{III}TMP(OH)$) belong to Fe^{III} high-spin complexes, the difference is that the CT state for the latter is higher than that for the former both in the visible (transition from $b_{2u}(\pi)$ and $a_{2u}(\pi)$ to $e_g(d\pi)$ in a D_{4h} notation) and in the near-IR ($a_{1u}(\pi)$ and $a_{2u}(\pi)$ to $e_g(d\pi)$) regions.[28-30,33,37] Although, little information was obtained on $Fe^{III}TMP$ dimers in the present study, their relation obtained from the electrochemical experiments[7,8] is included in the lower half of Scheme I. It is noteworthy that the spin state of $Fe^{III}TMP$ in solution phase is different from that in solid phase in the pH region of 6.5–11. Namely, solid samples obtained from solutions of pH 6.5–11 are low spin.[3,5]

The MCD behaviors of $Fe^{III}TMP(Im)_2$ and $Fe^{III}TMP(CN)_2$ are representative of Fe^{III} low-spin porphyrins throughout the UV to near-IR regions, while those of $Fe^{II}TMP(Im)_2$ and $Fe^{II}TMP(CN)_2$ are somewhat atypical for Fe^{II} low-spin complexes in that the Soret-band spectra are complicated and weak.

Acknowledgment. We thank Professor M. Hatano for use of the MCD apparatus. This research was partially supported by Grant-in-Aid for Scientific Research No. 57470105 from the Ministry of Education, Science and Culture in Japan.

Registry No. $Fe^{III}TMP$, 60489-13-6; $Fe^{II}TMP$, 71794-64-4; $Fe^{III}TMP(Im)_2$, 72595-74-5; $Fe^{II}TMP(Im)_2$, 87306-61-4; $Fe^{II}TMP(CN)_2$, 87306-62-5.

(47) N. Kobayashi and T. Osa, manuscripts in preparation.

Contribution from the Inorganic Chemistry Laboratory, University of Oxford, Oxford, U.K., and School of Chemical Sciences, University of East Anglia, Norwich NR4 7TJ, U.K.

Electronic Structure of Molybdenocene and Tungstenocene: Detection of Paramagnetism by Magnetic Circular Dichroism in Argon Matrices

P. ANTHONY COX,[1a] PETER GREBENIK,[1a] ROBIN N. PERUTZ,*[1a] MARK D. ROBINSON,[1a] ROGER GRINTER,[1b] and DAVID R. STERN[1b]

Received February 15, 1982

The magnetic circular dichroism (MCD) spectra are reported for WCp_2 and $MoCp_2$ (Cp = η-C_5H_5) generated in argon matrices by photolysis of MCp_2H_2. The spectra show a strong temperature dependence of intensity (*C* term), proving that these metallocenes are paramagnetic in their ground state. The photolysis of $W(MeCp)_2(C_2H_4)$ (MeCp = η-$C_5H_4CH_3$) in Ar matrices is reported to yield $W(MeCp)_2$. IR and UV data for $W(MeCp)_2$ are used to assist in assignments of absorptions of WCp_2. A method of analysis is developed in which spin–orbit coupling is treated as the dominant perturbation of the ground $^3E_{2g}$ state of the metallocenes. This method is applied to assign the infrared electronic absorptions of WCp_2 and $W(MeCp)_2$ to transitions between spin–orbit substates ($E_{1g} \leftarrow E_{2g}$). The spin–orbit coupling is shown to quench the dynamic Jahn–Teller effect in the ground state of WCp_2, but the off-diagonal Jahn–Teller term is much more significant for $MoCp_2$. The same method, used for the analysis of the MCD spectrum, shows that the sign and magnitude of $\Delta A/A$ (the ratio of the integrated differential absorption to the integrated absorption) for the lowest energy UV bands of both complexes are consistent with an $E_{2u} \leftarrow E_{2g}$ transition. This method sets a lower limit to $g_\parallel$ of 3.4 ± 0.7 (WCp_2) and 2.0 ± 0.2 ($MoCp_2$). Comparisons of the UV spectra of several metallocenes provide evidence that these are ligand-to-metal charge-transfer bands. It is shown that spin–orbit coupling lifts the symmetry restrictions on the reactivity of the d^4 metallocenes. The example of the paramagnetism of WCp_2 leads to the suggestion that paramagnetic intermediates may be important in many C–H insertion reactions.

Introduction

The metallocenes of molybdenum and tungsten have been postulated as intermediates in a number of reactions, most notably the C–H activation reactions of WCp_2H_2 and $WCp_2(CH_3)H$ (Cp = η-C_5H_5).[2] Recently, we described the characterization of these unstable metallocenes by matrix-isolation methods and have shown that they adopt a parallel sandwich structure.[3] Molybdenocene and tungstenocene were generated by photoelimination from $MCp_2(X)Y$ (X = Y = H, M = Mo, W; X = H, Y = CH_3, M = W) and MCp_2L (L = CO, M = Mo, W; L = C_2H_4, M = W) complexes and were characterized by IR and UV/vis spectroscopy. Notably, the IR spectrum of $MoCp_2$ resembled that of $CrCp_2$ in showing broad IR bands between 750 and 800 cm^{-1} and only one low-frequency skeletal mode. In accord with this, we postulated that $MoCp_2$ has an electronic ground state similar to that of $CrCp_2$, viz. a $^3E_{2g}$ state subject to both Jahn–Teller and spin–orbit effects. In contrast, WCp_2 showed a sharp IR spectrum with two low-frequency skeletal modes and an unusual electronic IR band at 3240 cm^{-1}. This difference was rationalized by the larger spin–orbit coupling constant of tungsten, which reduces the degeneracy of the ground state to a spin–orbit doublet (E_{2g}). The electronic IR band was assigned to an intraconfigurational vibronically allowed $E_{1g} \leftarrow E_{2g}$ transition.[3] (This corresponds to an $\Omega = 1 \leftarrow \Omega = 3$ transition in the closely related $C_{\infty v}$ point group, where Ω is

* To whom correspondence should be addressed at the Department of Chemistry, University of York, York Y01 5DD, U.K. No reprints available.

(1) (a) University of Oxford. (b) University of East Anglia.
(2) Berry, M.; Cooper, N. J.; Green, M. L. H.; Simpson, S. J. *J. Chem. Soc., Dalton Trans.* **1980**, 29. Berry, M.; Elmitt, K.; Green, M. L. H. *Ibid.* **1979**, 1950. Cooper, N. J.; Green, M. L. H.; Mahtab, R. *Ibid.* **1979**, 1557. Thomas, J. L.; Brintzinger, H. H. *J. Am. Chem. Soc.* **1972**, *94*, 1386. Thomas, J. L. *Ibid.* **1973**, *95*, 1838.
(3) Chetwynd-Talbot, J.; Grebenik, P.; Perutz, R. N. *Inorg. Chem.* **1982**, *21*, 3647.

0020-1669/83/1322-3614$01.50/0

the total angular momentum quantum number. However, we have found it misleading to treat these problems using the linear point group and will use the D_{5d} group exclusively.)

Magnetic circular dichroism (MCD) provides a powerful method of detecting paramagnetism, which is applicable under the conditions of matrix isolation to triplet and doublet states alike. For instance, it has been used by one of us to prove the paramagnetism of $Fe(CO)_4$.[4] We have also recorded the MCD spectra of some stable metallocenes of the first-row transition metals.[5] Both $MoCp_2$ and WCp_2 exhibit highly structured absorption bands in the near-UV spectrum. According to our postulate of a paramagnetic ground state, these bands should show a strong inverse temperature dependence of intensity when examined by MCD (C term). The lowest energy UV bands of WCp_2 and $MoCp_2$ show progressions of frequency 320 cm^{-1}, which were assigned to the symmetric ring–metal–ring stretching mode (ν_4, a_{1g}). In addition, each member of the progressions shows fine structure with splittings of 37–75 cm^{-1} that probably represents phonon coupling to the matrix in the excited state.

In this paper we report MCD experiments, which prove the paramagnetism of $MoCp_2$ and WCp_2 beyond reasonable doubt. We also report the synthesis of $W(MeCp)_2(C_2H_4)$ (MeCp = η-$C_5H_4CH_3$) and its photolysis in Ar matrices to give $W(MeCp)_2$. The electronic absorption spectra of $W(MeCp)_2$ are compared with those of WCp_2, so assisting in spectral assignments. In addition we examine in some detail the effects of spin–orbit coupling and Jahn–Teller distortions on the $^3E_{2g}$ manifold and show how their magnitudes affect both the electronic ground state and the reactivity of the d^4 metallocenes. The magnitude of the MCD C terms is analyzed in terms of the symmetries of the ground and excited states.

Experimental Section

MCD. The precursor complexes, MCp_2H_2 (M = Mo, W), prepared as described elsewhere,[6] were sublimed into a glass tube that was sealed in vacuo. Immediately before use, the tip of the tube was broken and the tube inserted into a furnace, which was attached to the vacuum shroud of the matrix/MCD apparatus. Sublimation temperatures have been listed earlier.[3] The design of the furnace and the matrix/MCD equipment has also been described.[7] The precursor complexes were codeposited with research grade argon (Messer-Griesheim) onto a sapphire window. The matrices were clear visually; the quality of the MCD spectra recorded indicates minimal depolarization by the matrix. UV spectra were recorded on a Cary 17D spectrophotometer after deposition and after photolysis. MCD measurements were then made on the same samples by using a Cary 61 dichrograph. The matrices were photolyzed with use of a water-filtered Philips HPK 125-W mercury arc.

$W(MeCp)_2(C_2H_4)$. WCl_6 was converted to $W(MeCp)_2H_2$ by the same route as for WCp_2H_2.[6] However, it proved photostable in matrices and in solution. It was converted to $W(MeCp)_2Cl_2$ and reacted with $EtAlCl_2$ to form red-orange $W(MeCp)_2(C_2H_4)$ following the procedure of Benfield and Green.[8] $W(MeCp)_2(C_2H_4)$ was characterized by ^1H NMR at 300 MHz in C_6D_6 (δ 3.89, 3.58 (multiplet, 8 H, C_5H_4), 1.89 (singlet, 6 H, CH_3), 0.80 (singlet with satellites, J_{WH} = 5.2 Hz, 4 H, C_2H_4)), by its mass spectrum (m/e 370 (M^+), 342 ($M^+ - C_2H_4$); values given for ^{184}W), and by IR after sublimation (335–345 K) into Ar matrices at 20 K (3054, 2985, 2960, 2929, 2898, 1465, 1460, 1449, 1441, 1421, 1382, 1375, 1370, 1363, 1227, 1112, 1036, 1031, 1019, 1007, 932, 885, 867, 848, 841, 443, 399, 385, 375, 347 cm^{-1}). Its UV/vis spectrum in Ar matrices showed bands at 286 and 245 nm with a long tail extending into the visible region. The conditions of matrix isolation are described elsewhere.[3]

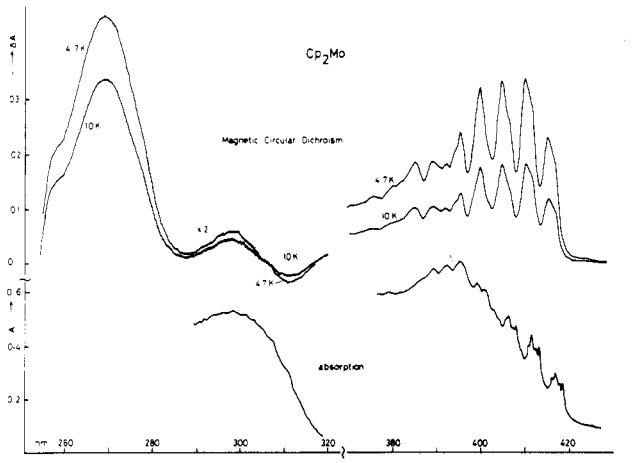

Figure 1. Bottom: UV absorption spectra of $MoCp_2$ in Ar at 10 K obtained after 105-min deposition of $MoCp_2H_2$ and Ar and 30-min subsequent photolysis. Top: MCD spectra of the same matrix at 10 K and after cooling to 4.7 K (field 0.34 T).

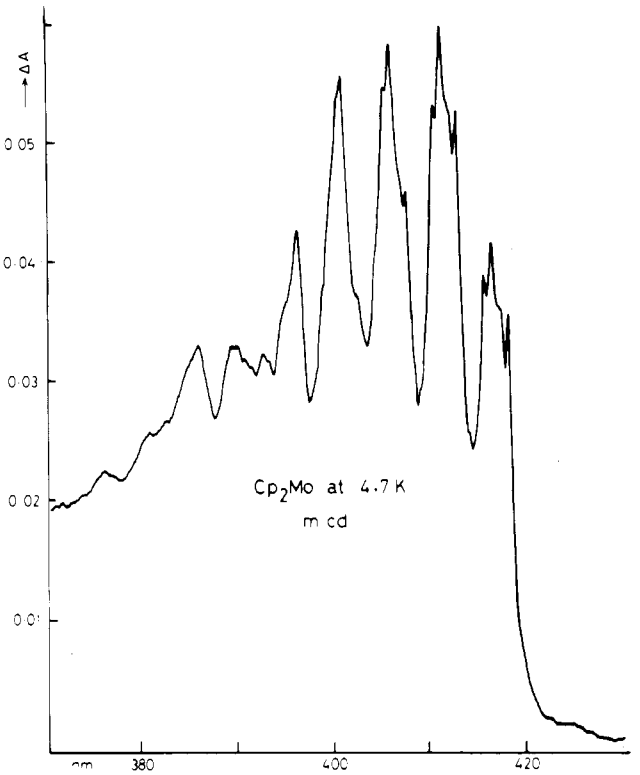

Figure 2. MCD of the lowest energy absorption of $MoCp_2$ at 4.7 K under higher resolution (slit 0.3 nm; other conditions as in Figure 1).

Results

MCD of $MoCp_2$ and WCp_2. Figure 1 shows the UV absorption spectrum and temperature-dependent MCD spectrum of $MoCp_2$ generated by photolysis of $MoCp_2H_2$ in an Ar matrix at 12 K. The structured MCD band at 400 nm is shown under higher resolution in Figure 2 and reveals splittings as small as 0.7 nm. Figure 3 shows the lowest energy absorption band and corresponding MCD spectrum of WCp_2 together with its temperature dependence, obtained by photolysis of WCp_2H_2 in Ar. The absorption spectra are in excellent agreement with those measured previously.[3] The spectra of $MoCp_2$ are better resolved than in our previous measurements, perhaps because of the lower temperature employed. Comparison of the absorption spectra and MCD

(4) Barton, T. J.; Grinter, R.; Thomson, A. J.; Davies, B.; Poliakoff, M. *J. Chem. Soc., Chem. Commun.* **1977**, 841.
(5) Barton, T. J.; Grinter, R.; Thomson, A. J. *J. Chem. Soc., Dalton Trans.* **1979**, 1912.
(6) Green, M. L. H.; Knowles, P. J. *J. Chem. Soc., Perkin Trans. 1* **1973**, 989.
(7) Barton, T. J.; Grinter, R.; Thomson, A. J. *J. Chem. Soc., Dalton Trans.* **1978**, 608.
(8) Benfield, F. W. S.; Green, M. L. H. *J. Chem. Soc., Dalton Trans.* **1974**, 1324.

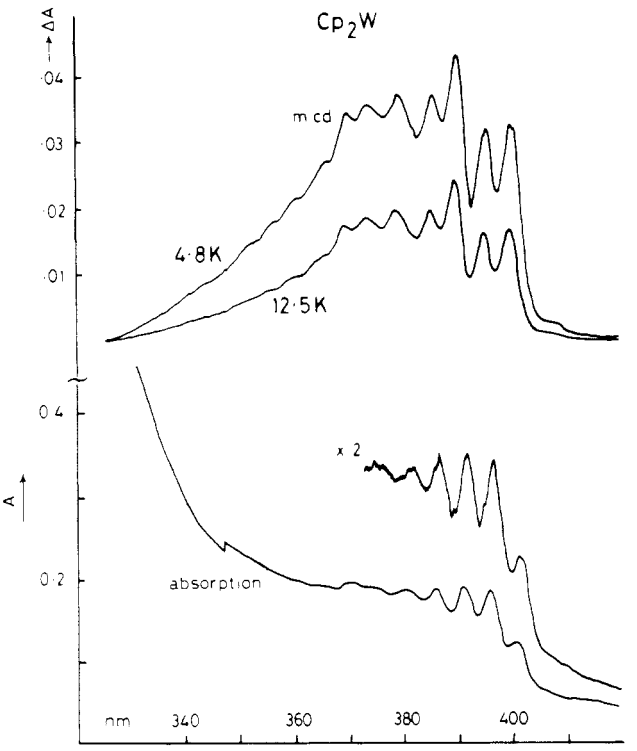

Figure 3. Bottom: UV absorption spectra of WCp_2 in Ar at 12.5 K obtained following 45-min deposition of WCp_2H_2 and Ar at 15 K and 30-min subsequent UV photolysis. Top: MCD spectra of the same region at 12.5 K and after cooling to 4.8 K (field 1.7 T).

Table I. Magnetic Circular Dichroism and UV Absorption of WCp_2 and $MoCp_2$ (nm)

WCp_2		$MoCp_2$	
MCD[a]	abs[b]	MCD[a]	abs[b,c]
400.8 (+)	400.6	416.9 (+)	416.9
395.8 (+)	395.7	411.9 (+)	411.7
390.8 (+)	391.1	406.6 (+)	406.5
386.4 (+)	386.0	401.6 (+)	401.0
380.1 (+)	381.0		399.4
374.9 (+)	375.0	395.9 (+)	396.0
370.8 (+)	371.0	393.5 (+)	393.0
365.1 (+)		389.4 (+)	
360.9 (+)		385.6 (+)	
	323	360 (sh) (+)	
273 (+)	*d*	312 (−)	
244 (+)	*d*	300 (+)	301
244 (−)	*d*	270 (+)	*d*

[a] The sign of ΔA is given in parentheses. [b] Data from ref 3. [c] The first three members of this progression were each split into four components in the experiments reported here. The most intense component (the third) was coincident with that recorded in ref 3. The four components of the first band were at 418.7, 418.0, 416.9, and 416.2 nm. [d] Obscured by precursor absorptions.

spectra (Table I) shows without doubt that the low-energy MCD absorption bands must be assigned to the metallocenes. All of the MCD spectra show a strong, reversible, inverse temperature dependence of intensity, demonstrating that they arise from a species with a paramagnetic ground state. It is hard to detect absorption bands of the metallocenes in the 200–300-nm region, because of the dominant absorption of the precursors. However, the MCD spectra show several *C*-term bands in this region that must also be assigned to the metallocenes (Figure 4). Since the separations of the progression components of the lowest energy band differed from those measured in the absorption spectrum by <0.5 nm, we conclude that any contribution from *A* terms of derivative shape to the MCD spectrum is negligible. Indeed, this is what

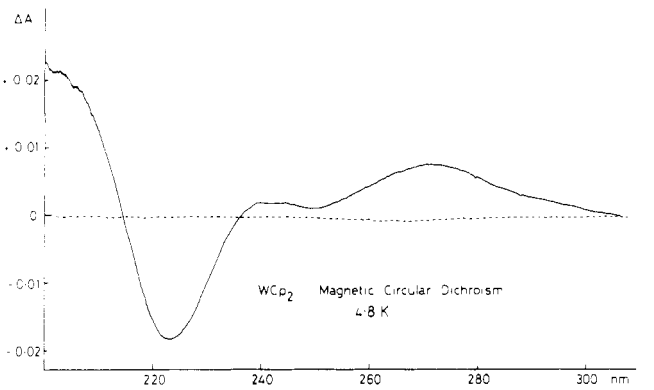

Figure 4. MCD spectrum (full line) of WCp_2 in Ar at 4.7 K below 350 nm (field 5.3 T; other conditions as in Figure 3). Note that the spectrum at 6.5 T was almost superimposable, because of saturation. The broken line shows the experimental base line.

would be anticipated at such low temperatures, where the *C* terms dominate any other contribution to the MCD spectrum.

The low-temperature spectra shown in Figures 1 and 2 were taken under relatively low-field conditions (0.34 T). At higher field the MCD of $MoCp_2$ was so intense that it exceeded the maximum ellipticity that the instrument could measure. In the case of WCp_2, the MCD spectrum of Figure 4 was close to field saturation at 4.7 K and 5.3 T. Using the spectra at 10–12.5 K where saturation should present no problem, we have estimated the ratios of integrated differential absorption to integrated absorption as $\Delta A/A(WCp_2) = 0.31 \pm 0.08$ at 1.7 T and $\Delta A/A(MoCp_2) = 0.048 \pm 0.005$ at 0.34 T.

Generation of $W(MeCp)_2$. Argon matrices containing $W(MeCp)_2(C_2H_4)$ were examined by IR and UV/vis absorption spectroscopy before and after photolysis. UV photolysis caused a decrease in intensity of the precursor bands and growth of new IR bands at 3099, 1439, 951, and 938 cm^{-1}, which may be assigned to expelled ethylene.[3,9] Further IR product bands were detected at 3227 (broad), 1215, 1031, 1016, 789, and 764 cm^{-1}, of which the first was the most intense. The presence of this band so close to the IR electronic transition of WCp_2 at 3240 cm^{-1} indicates that these bands should be assigned to $W(MeCp)_2$. Although further IR bands would be expected for $W(MeCp)_2$, they have not yet been identified because of overlap with precursor absorptions and lack of intensity. UV absorption spectra showed the growth on photolysis of $W(MeCp)_2(C_2H_4)$ in Ar of an intense absorption due to $W(MeCp)_2$ with components at 417 (shoulder), 407, and 395 nm. The first component of this band is shifted 15 nm (920 cm^{-1}) to the red relative to the prominent low-energy absorption of WCp_2.

Analysis and Discussion

In the following discussion we start by examining the effect of spin–orbit coupling on the electronic ground state of the d^4 metallocenes. We then consider the effect of Jahn–Teller coupling as a perturbation of the spin–orbit states. The results are used to rationalize the vibrational and electronic IR spectra of the metallocenes. Subsequently, we present an analysis of the MCD spectra, with a view to determining the symmetry of the upper electronic states and obtaining information about the ground-state magnetic properties. Finally, we examine the influence of spin–orbit coupling on symmetry control of reactivity of the metallocenes. Our approach contrasts with that used by Ammeter for first-row d^5 systems, which assumes that Jahn–Teller effects dominate.[10]

(9) Barnes, A. J.; Howells, J. D. R. *J. Chem. Soc., Faraday Trans. 2* **1973**, *69*, 532.
(10) Ammeter, J. H.; Zoller, L.; Bachmann, J.; Baltzer, P.; Gamp, E.; Bucher, R.; Deiss, E. *Helv. Chim. Acta* **1981**, *64*, 1063.

Table II. Effect of Spin-Orbit Coupling on the $^3E_{2g}$ and $^1E_{2g}$ Wave Functions

spin-orbit wave function[a]	symmetry	energy	total angular momentum (Ω)
F_{1a} $\|E_{2+}\alpha\alpha\rangle$	E_{2g}	$-(8B + \zeta)$	3
F_{1b} $\|E_{2-}\beta\beta\rangle$	E_{2g}	$-(8B + \zeta)$	−3
F_{2a} $\|E_{2+}(\alpha\beta + \beta\alpha)\rangle$	E_{2g}	$-(64B^2 + \zeta^2)^{1/2}$	2
F_{2b} $\|E_{2-} - (\alpha\beta + \beta\alpha)\rangle$	E_{2g}	$-(64B^2 + \zeta^2)^{1/2}$	−2
F_{3a} $\|E_{2+}\beta\beta\rangle$	E_{1g}	$-8B + \zeta$	1
F_{3b} $\|E_{2-}\alpha\alpha\rangle$	E_{1g}	$-8B + \zeta$	−1
F_{4a} $\|E_{2+}(\alpha\beta - \beta\alpha)\rangle$	E_{2g}	$(64B^2 + \zeta^2)^{1/2}$	2
F_{4b} $\|E_{2-} - (\alpha\beta - \beta\alpha)\rangle$	E_{2g}	$(64B^2 + \zeta^2)^{1/2}$	−2

[a] The spin functions represent holes rather than electrons.

Effect of Spin–Orbit Coupling. The $^3E_{2g}$ ground state of the d^4 metallocenes and its associated singlet arise from the configuration $a_{1g}{}^1e_{2g}{}^3$. The effect of spin–orbit coupling on the $^3E_{2g}$ term has been described elsewhere,[11] but without consideration of the mixing of the singlet and triplet states that becomes important with the heavy metals. We use the complex orbital functions $|E_{2g+}\rangle$ and $|E_{2g-}\rangle$; use of the D_{5d} character table shows that they transform as follows under rotation and reflection operations:

$$\hat{C}_5|E_{2g\pm}\rangle = e^{\pm 4\pi i/5}|E_{2g\pm}\rangle \qquad \sigma_d|E_{2g+}\rangle = |E_{2g-}\rangle$$

From these functions, the four pairs of spin–orbit functions listed in Table II are generated (see also Figure 11 of ref 3 for a plot of their energy variations). The triplet and singlet functions are separated initially by $16B$ (B is the Racah electron repulsion parameter), while the spin–orbit coupling splits the triplet into three doubly degenerate pairs of levels separated by ζ.[12] However, the off-diagonal spin–orbit element mixes F_2 and F_4 very substantially when the spin–orbit coupling constant, ζ, becomes large.

In our earlier paper, we postulated that the electronic IR band represents a vibronic transition from F_1 to F_3, with energy $2\zeta + \nu$ where ν is the frequency of the allowing mode. A vibronic transition from the ground spin–orbit doublet is possible if the appropriate matrix elements are nonzero. This condition will be satisfied by the elements

$$\langle E_{2g+}\alpha\alpha\ (v = 0)|\mathbf{m}|E'_{2g-}\alpha\alpha\ (v = 1)\rangle$$
$$\langle E_{2g-}\beta\beta\ (v = 0)|\mathbf{m}|E'_{2g+}\beta\beta\ (v = 1)\rangle$$

(where $E_{2g\pm}$ represents F_1, $E'_{2g\pm}$ represents F_3, $\mathbf{m}$ is the dipole moment operator, and the spin functions represent holes rather than electrons), provided that the enabling vibration has symmetry e_{2u}, e_{1u}, a_{1u}, or a_{2u}. The most likely modes are the skeletal vibrations $\nu_{11}(a_{2u})$, $\nu_{21}(e_{1u})$, or $\nu_{22}(e_{1u})$ that fall below 350 cm^{-1}. No other transition is possible from F_1 without violating spin-orthogonality conditions. Assigning the electronic IR transitions of tungstenocene to such a transition, we estimated ζ for WCp_2 to be in the range 1450–1570 cm^{-1}. On substitution of the η-C_5H_5 ring by η-C_5H_4Me, we would anticipate a marginal reduction in ζ because of the improved overlap with the metal and a small change in the frequency of the allowing mode. In accord with this prediction, the IR electronic band of $W(MeCp)_2$ is shifted only 13 cm^{-1} to lower wavenumbers from that of WCp_2 when generated from $WCp_2(C_2H_4)$.[3]

Effect of Jahn–Teller Coupling. It is now appropriate to examine the effect of the Jahn–Teller Hamiltonian on each of the spin–orbit components. Since the Jahn–Teller-active mode appropriate to a $^3E_{2g}$ state has e_{1g} symmetry, we may write the Jahn–Teller Hamiltonian as[13]

$$\hat{H}_{JT} = (\partial H/\partial Q_+)Q_+ + (\partial H/\partial Q_-)Q_-$$

where $Q_\pm$ are the complex combinations of the e_{1g} normal coordinates with the following transformation properties:

$$\hat{C}_5Q_\pm = e^{\pm 2\pi i/5}Q_\pm \qquad \sigma_dQ_+ = Q_-$$

The matrix elements of the Jahn–Teller operator acting on the orbital part of the E_{2g} wave function have the form

$$\langle E_{2g\rho}|\partial H/\partial Q_\sigma|E_{2g\tau}\rangle$$

where $\rho = \pm 1$, $\tau = \pm 1$, and $\sigma = \pm 1$. Under a C_5 rotation this element is transformed into

$$e^{2\pi i(-2\rho+\sigma+2\tau)/5}\langle E_{2g\rho}|\partial H/\partial Q_\sigma|E_{2g\tau}\rangle$$

For a nonzero element in $\hat{H}_{JT}$ connecting the components of F_1, this element must be totally symmetric (i.e., we must conserve orbital angular momentum), implying that

$$-2\rho + \sigma + 2\tau = 0, \pm 5$$

This requirement is satisfied only if $\tau = 1$, $\sigma = 1$, and $\rho = -1$ or if $\tau = -1$, $\sigma = -1$, and $\rho = 1$, implying that the only two elements involving F_1 only, which are nonzero, are

$$\langle E_{2g-}|\partial H/\partial Q_+|E_{2g+}\rangle \qquad \langle E_{2g+}|\partial H/\partial Q_-|E_{2g-}\rangle$$

Remembering that $\hat{H}_{JT}$ leaves the spin functions unaffected, we see that there are no nonzero elements connecting F_{1a} with F_{1b} or F_{3a} with F_{3b}. On the other hand, there are no spin restrictions on the elements connecting the pairs F_{2a}, F_{2b} and F_{4a}, F_{4b}. It follows that only F_2 and F_4 are subject to the diagonal Jahn–Teller effect. However, with the same type of argument, there *are* nonzero off-diagonal Jahn–Teller elements connecting the pairs of states F_{1a}, F_{3b} and F_{1b}, F_{3a}. Since these states are separated by an energy 2ζ, a competition results between the spin–orbit coupling and the off-diagonal Jahn–Teller effect, both of which act on the ground doublet F_1.

Application to the Metallocenes. We now examine how the spin–orbit and Jahn–Teller effects will influence the ground states of the metallocenes. In the case of tungstenocene, we estimate $\zeta \sim 1500$ cm^{-1} and $B \sim 200$ cm^{-1}, implying substantial spin–orbit mixing of the triplet and singlet functions. The separation of F_1 and F_2 is estimated as $\sim$900 cm^{-1} before considering Jahn–Teller effects. The IR spectra of WCp_2 at 20 K suggest that the ground state is a simple doublet with no significant Jahn–Teller distortions, implying that the spin–orbit stabilization of F_1 has quenched the off-diagonal Jahn–Teller effect. However, at higher temperatures we would anticipate population of the Jahn–Teller distorted F_2 doublet.

The values of ζ and B for $MoCp_2$ should be about 500 and 300 cm^{-1}, respectively, so there should be little spin–orbit mixing of singlet and triplet components. The separation of F_1 and F_2 has now dropped to $\sim$350 cm^{-1}, neglecting any Jahn–Teller stabilization. The IR spectra suggest a major role for the Jahn–Teller effect. This may be understood either if F_2 has fallen below F_1 in energy or if the off-diagonal stabilization of F_1 has become significant because of the low spin–orbit coupling constant.

The case of chromocene is probably treated best by different methods that assume that the Jahn–Teller effect has the dominant role. Estimating ζ as 150 cm^{-1} and B as 500 cm^{-1},[12] we calculate that F_1 and F_2 are separated by only 150 cm^{-1} before we consider the Jahn–Teller stabilization. An electronic band has been observed in the low-temperature Raman

(11) (a) Parameswaran, T.; Koningstein, J. A.; Haley, L. V.; Aleksanyan, V. T. *J. Chem. Phys.* **1978**, *68*, 1285. (b) Brintzinger, H. H.; Lohr, L. L.; Wong, K. L. T. *J. Am. Chem. Soc.* **1975**, *97*, 5146.
(12) Warren, K. D. *Struct. Bonding (Berlin)* **1976**, *27*, 45.
(13) Longuet-Higgins, H. C.; Öpik, U.; Pryce, M. H. L.; Sack, R. A. *Proc. R. Soc. London, Ser. A* **1958**, *244*, 1.

spectrum of solid $CrCp_2$ at ~280 cm^{-1},[11a] which has been assigned to a transition between states of a C_5-distorted molecule, correlating with F_1 and F_3. Unfortunately, neither the details of the Jahn–Teller effect nor the possibility of cooperative effects in the crystal appear to have been considered.

Analysis of MCD Spectra. The experimental MCD and absorption spectra give us the magnitude and sign of $\Delta A/A$ for the lowest energy transition. The theoretical value of $\Delta A/A$ for a randomly oriented set of molecules depends on the symmetries of both ground and excited states. For the ground-state wave functions we use F_{1a} and F_{1b} (Table II). The estimates of the extinction coefficient of the lowest energy band (~10^3 dm^3 mol^{-1} cm^{-1}) suggested that this is an allowed charge-transfer transition from the $^3E_{2g}$ ground state, implying excited-state symmetries E_{1u} (x,y polarized) or E_{2u} (with both x,y and z components). We also consider the less likely possibility of a $^3A_{2g}$ ground state. According to Stephens[14] the magnitudes of the C (MCD) and D (absorption) terms for a randomly oriented system are given by

$$C = \frac{1}{2d_a}\sum_{\alpha,\alpha',\lambda} \mathrm{Im}\{\langle\alpha|\mathbf{m}|\lambda\rangle \times \langle\lambda|\mathbf{m}|\alpha'\rangle\cdot\langle\alpha'|\mu|\alpha\rangle\} \quad (1)$$

$$D = \frac{1}{d_a}\sum_{\alpha,\lambda}\langle\alpha|\mathbf{m}|\lambda\rangle^2 \quad (2)$$

where α and α' are the two components of the ground-state wave function, λ is the excited-state wave function, μ is the magnetic dipole operator, $\mathbf{m}$ is the electric dipole operator, and d_a is the degeneracy of the ground state. In order to employ our complex wave functions, we represent $\mathbf{m}$ in its complex form:

$$m_0 = m_z$$

$$m_+ = 1/2^{1/2}(-im_x + m_y)$$

$$m_- = 1/2^{1/2}(im_x + m_y)$$

Similarly, μ is converted to μ_0, μ_+, and μ_-. These operators transform as the following irreducible representations:

$$m_0\colon a_{2u} \qquad m_\pm\colon e_{1u} \qquad \mu_0\colon a_{2g} \qquad \mu_\pm\colon e_{1g}$$

We will make use of the transformation properties under C_5 and $\sigma_d(yz)$ to determine which matrix elements are nonzero (these have already been mentioned for e_{1u} and e_{2g} representations). It should be noted that $\mathbf{m}$ and μ differ in their transformation under reflection since $\mathbf{m}$ transforms as a polar vector while μ transforms as an axial vector.

The expression for C can be simplified considerably by evaluating the matrix elements involving μ at this stage. Use of the symmetries with respect to reflection and Slater determinantal wave functions $|0\bar{2}-2-\bar{2}|$ and $|02\bar{2}-2|$ for the ground state (E_{2g+} and E_{2g-}, respectively) shows that

$$\langle E_{2g+}|\mu_0|E_{2g+}\rangle = -\langle E_{2g-}|\mu_0|E_{2g-}\rangle = 4\beta$$

$$\langle E_{2g+}|\mu_0|E_{2g-}\rangle = \langle E_{2g\pm}|\mu_\pm|E_{2g\pm}\rangle = 0$$

where β is the Bohr magneton; i.e., $g_\parallel = 4$ and $g_\perp = 0$ in accord with Warren's results.[12]

The transformation above may now be applied to C and D and the results simplified to

$$C = \frac{1}{4}\sum_{\alpha,\alpha',\lambda}\mu_0^{\alpha\alpha'}(m_+^{\alpha\lambda}m_-^{\lambda\alpha'} - m_-^{\alpha\lambda}m_+^{\lambda\alpha'}) \quad (3)$$

$$D = \frac{1}{2}\sum_{\alpha,\lambda}(m_+^{\alpha\lambda}m_-^{\lambda\alpha} + m_-^{\alpha\lambda}m_+^{\lambda\alpha} + m_0^{\alpha\lambda}m_0^{\lambda\alpha}) \quad (4)$$

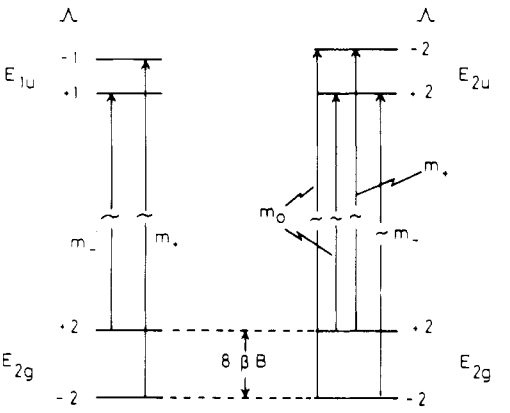

Figure 5. Energy-level diagram showing the allowed MCD transitions for the E_{2g} spin–orbit ground state of WCp_2 derived from the $^3E_{2g}$ manifold.

where $m_+^{\alpha\lambda} = \langle\alpha|m_+|\lambda\rangle$ etc. These equations are valid provided that all the matrix elements are real.

Starting with the transition to an E_{1u} excited state, we identify the nonzero elements in $m_\pm$ using the $\hat{C}_5$ and $\hat{\sigma}_d$ operators as we did for the Jahn–Teller coupling:

$$\langle E_{2g+}|m_+|E_{1u+}\rangle = \langle E_{2g-}|m_-|E_{1u-}\rangle = \langle E_{1u+}|m_-|E_{2g+}\rangle = \langle E_{1u-}|m_+|E_{2g-}\rangle = m$$

where m is a constant. Substituting into eq 3 and 4, we obtain

$$C = 2\beta m^2 \qquad D = m^2 \qquad C/D = 2\beta$$

For the transition to an E_{2u} excited state, we define two electric dipole matrix elements, $m_\parallel$ and $m_\perp$, and use the $\hat{C}_5$ and $\hat{\sigma}_d$ operators again to identify the following nonzero matrix elements:

$$\langle E_{2g-}|m_+|E_{2u+}\rangle = \langle E_{2g+}|m_-|E_{2u-}\rangle = \langle E_{2u-}|m_+|E_{2g+}\rangle = \langle E_{2u+}|m_-|E_{2g-}\rangle = m_\perp$$

$$\langle E_{2g+}|m_0|E_{2u+}\rangle = \langle E_{2g-}|m_0|E_{2u-}\rangle = \langle E_{2u+}|m_0|E_{2g+}\rangle = \langle E_{2u-}|m_0|E_{2g-}\rangle = m_\parallel$$

Substituting into eq 3 and 4 we obtain

$$C = -2\beta m_\perp^2 \qquad D = (m_\parallel^2 + m_\perp^2)$$

$$C/D = -2\beta m_\perp^2/(m_\parallel^2 + m_\perp^2)$$

Thus, we predict that the C terms should have opposite signs for E_{1u} and E_{2u} excited states and that C/D should be 2β for E_{1u} but $\leq 2\beta$ for E_{2u} excited states (Figure 5). If delocalization onto the ligands is considered, these figures should be reduced by a factor of $(1 + k)/2$, where k is the orbital reduction factor.

In principle, there is a possibility that the d^4 metallocenes have a $a_{1g}^2e_{2g}^2$ ($^3A_{2g}$) ground state. The zero-field effect splits this state into A_1, which is nonmagnetic, and E_1 states. We may assume that the zero-field splitting is much greater than Zeeman splitting and that only one of the zero-field states will be significantly populated at low temperature (cf. ZFS of $NiCp_2$ = 26 cm^{-1}).[15] The values for C/D may be evaluated as previously and are given together with those for the $^3E_{2g}$ ground state in Table III.

We may now compare our experimental results with the theoretical predictions. The relationship between C/D and $\Delta A/A$ is[14]

$$\frac{C}{D} = -1.072\frac{kT}{B}\frac{\Delta A}{A}\mu_B$$

where B is in tesla and k in cm^{-1} K^{-1}. For the lowest energy

(14) Stephens, P. J. *Annu. Rev. Phys. Chem.* **1974**, *25*, 201.

(15) Prins, R.; Van Voorst, J. D. W. *J. Chem. Phys.* **1968**, *49*, 4665.

Table III. Predictions of C/D according to the Symmetries of Ground and Excited States

lower manifold	spin-orbit state: lower	spin-orbit state: upper	calcd C/D
$^3E_{2g}$	E_{2g}	E_{1u}	2β
$^3E_{2g}$	E_{2g}	E_{2u}	$-2\beta m_\perp^2/(m_\parallel^2 + m_\perp^2)$
$^3A_{2g}$	A_{1g}	A_{2u}, E_{1u}	no C term
$^3A_{2g}$	E_{1g}	E_{1u}	no C term
$^3A_{2g}$	E_{1g}	E_{2u}	$+\beta$
$^3A_{2g}$	E_{1g}	A_{2u}	$-\beta$
$^3A_{2g}$	E_{1g}	A_{1u}	$-\beta$

Table IV. Lowest Energy Charge-Transfer Bands of Neutral Metallocenes (cm^{-1})

d^6	$FeCp_2$[a]	38 200	$RuCp_2$[b]	42 000	$OsCp_2$	
d^5	$Mn(MeCp)_2$[a,c]	24 400	$TcCp_2$		$ReCp_2$[d]	200 80
d^4	$CrCp_2$[a]	29 600	$MoCp_2$[e]	23 980	WCp_2[e]	249 60

[a] From ref 16. [b] From ref 12. [c] Low spin. [d] From ref 21. [e] From ref 3.

absorption bands of WCp_2 and $MoCp_2$ we obtain $C/D(WCp_2) = -1.70 \pm 0.4$ and $C/D(MoCp_2) = -1.04 \pm 0.1$ μ_B. The substantial C term for WCp_2 argues strongly against a $^3A_{2g}$ ground state, regardless of the sign of the zero-field splitting. On the other hand, the magnitude of C/D for WCp_2 is entirely consistent with our analysis for the F_1 component of the $^3E_{2g}$ ground state. The value can be accounted for by a $E_{2u} \leftarrow E_{2g}$ transition and an orbital reduction factor $k = 0.7$ with only a slight parallel contribution to the transition moment. The magnitude of C/D for $MoCp_2$ is significantly lower than for tungsten, but the sign is unchanged, suggesting that we are dealing with the same type of transition. This reduction could represent a larger parallel contribution than for tungsten or more likely a lower value of $g_\parallel$. If the Jahn–Teller effect plays a significant role for $MoCp_2$ as we have argued above, we would indeed expect mixing into the ground state of F_3 which has $g_\parallel = 2(1 - k)$.[12] From this analysis we may deduce, therefore, lower limiting values of $g_\parallel$ of 3.4 (WCp_2) and 2.1 ($MoCp_2$).

Direction of Charge Transfer. Although the analysis of the MCD spectra specifies the symmetry of the upper state involved in the low-energy UV absorption of the metallocenes as E_{2g}, this does not distinguish a metal-to-ligand (MLCT) from a ligand-to-metal charge-transfer (LMCT) transition.[12] Nevertheless, there are two arguments that strongly suggest a LMCT transition. The first is derived by consideration of the energies of the first charge-transfer transitions of neutral d^4–d^6 metallocenes (Table IV). Whereas the first CT band of the d^6 metallocenes lies above 35 000 cm^{-1}, the d^5 (low spin) metallocenes show bands at 20 000–25 000 cm^{-1} and the d^4 metallocenes at 24 000–30 000 cm^{-1}. This major reduction in energy is readily understood by the creation of holes in the $a_{1g}^2e_{2g}^4$ configuration of the d^6 species, but there is no reason to anticipate such gross changes in MLCT transitions. The second argument is based on the small red shifts in the first CT band observed with the $M(MeCp)_2$ complexes.[16] The inductive effect of the methyl groups is expected to shift the ligand levels to high energy, resulting in a red shift of LMCT and a blue shift of MLCT bands. This postulate is supported by the consistent decrease in the energy separation of the d levels and the highest occupied ligand levels found when comparing photoelectron spectra of MCp_2 and $M(MeCp)_2$ complexes.[17] From this argument, the first CT bands of all the stable metallocenes have been assigned as LMCT transitions.[16] The comparable red shift (920 cm^{-1}) observed for $W(MeCp)_2$ relative to WCp_2 would lead to the same assignment. However, we note that this method is based on a one-electron approximation and would be susceptible to error if configuration interaction changed appreciably on methylation. Three groups of LMCT bands are anticipated:

$$e_{1u} \rightarrow e_{2g} \qquad {}^3E_{2g} \rightarrow {}^{1,3}E_{1u}$$

$$e_{1u} \rightarrow a_{1g} \qquad {}^3E_{2g} \rightarrow {}^{1,3}E_{1u} + {}^{1,3}E_{2u}$$

Since both $^3E_{1u}$ and $^3E_{2u}$ terms give rise to E_{2u} spin–orbit states, it is not possible to identify the LMCT transition in detail. The higher energy bands may be assigned to E_{2u} excited states (positive MCD term) or E_{1u} excited states (negative MCD term), but this does not allow a full assignment of these transitions either.

Symmetry Control of Reactivity. Veillard has demonstrated that the thermal reaction of d^4 metallocenes with CO to form MCp_2CO (M = Cr, Mo, W) is symmetry forbidden if spin–orbit effects are neglected.[18] However, these reactions occur at temperatures as low as 60 K for $MoCp_2$ and WCp_2[3] and at <195 K for $CrCp_2$.[19] If the effect of spin–orbit coupling is considered, the ground state transforms as E_{2g} under D_{5d} symmetry but as $A_1 + B_2$ under C_{2v} symmetry as appropriate to MCp_2CO. It is then clear that spin–orbit coupling causes a direct correlation between MCp_2 and the $^1A_1$ ground state of MCp_2CO. We consider, therefore, that symmetry restrictions on reactivity are not of critical importance and that spin–orbit coupling provides a mechanism for intersystem crossing.

Conclusions

The MCD experiments reported in this paper provide positive evidence for the paramagnetism of $MoCp_2$ and WCp_2. The observation of field saturation of the MCD spectra strongly suggests a major orbital contribution. Moreover, the analysis of the C term of WCp_2 strongly favors an E_{2g} ground state arising from the effect of spin–orbit coupling on a $^3E_{2g}$ term. The estimates of $\Delta A/A$ are used to obtain lower limiting values of $g_\parallel$ of 3.4 and 2.1 for WCp_2 and $MoCp_2$, respectively. The lowest energy UV absorption is identified as an $E_{2u} \leftarrow E_{2g}$ LMCT transition. Detailed analysis of the ground state shows that the spin–orbit coupling quenches the Jahn–Teller effect in WCp_2 but that the Jahn–Teller effect and spin–orbit coupling compete in $MoCp_2$.

The methods developed in this paper apply to metallocenes with E_{2g} ground states in which spin–orbit coupling exceeds Jahn–Teller effects. In addition to the d^4 systems, these methods could be applied to the hypothetical d^2 metallocenes $ZrCp_2$ and $HfCp_2$ by reversing the order of the spin–orbit functions. They could also be applied with very little change to d^5 metallocenes with $^2E_{2g}$ ground states (e.g., $[Os(MeCp)_2]^+$ and perhaps $ReCp_2$).[20,21]

Parshall pointed out that an effective C–H activator should have a high-lying donor *and* a low-lying acceptor orbital, which must carry two electrons between them.[22] He also indicated that this conclusion raised the question of whether the intermediate is a triplet or a singlet. In our previous study, we demonstrated that the C–H-activating intermediate in the $WCp_2(X)Y$ systems is almost certainly WCp_2.[3] In the present

(16) Gordon, K. R.; Warren, K. D. *Inorg. Chem.* **1978**, *17*, 987.
(17) Green, J. C. *Struct. Bonding (Berlin)* **1981**, *43*, 37.
(18) Veillard, A. *Nouv. J. Chim.* **1981**, *5*, 599. Our objections appear to have been met in a new paper (Veillard, A.; Dedieu, A., to be submitted for publication), which ascribes the apparent symmetry violations to the effect of spin–orbit coupling.
(19) Wong, K. L. T.; Brintzinger, H. H. *J. Am. Chem. Soc.* **1975**, *97*, 5143.
(20) Evans, S.; Green, M. L. H.; Jewitt, B.; Orchard, A. F.; Pygall, C. F. *J. Chem. Soc., Faraday Trans. 2* **1972**, *68*, 1847.
(21) Chetwynd-Talbot, J.; Grebenik, P.; Perutz, R. N. *J. Chem. Soc., Chem. Commun.* **1981**, 452. Chetwynd-Talbot, J.; Grebenik, P.; Perutz, R. N.; Powell, M. H. A. *Inorg. Chem.* **1983**, *22*, 1675.
(22) Parshall, G. W. *Spec. Period. Rep.: Catalysis* **1977**, *1*.

work, we have proved the paramagnetism of WCp_2. As our experiments showed,[3] the two unpaired electrons need not pose a bar to reactivity, because the large spin–orbit coupling constants of the heavy metals provide a mechanism of intersystem crossing. On the contrary, their presence may be conducive to C–H activation. In future experiments, it will be important to test for paramagnetism in other C–H-activating intermediates.

Acknowledgment. Both the Norwich and the Oxford groups acknowledge support from the SERC. The Norwich group also thanks the Royal Society for financing the cryostat. P.G. thanks British Petroleum and St. Anne's College, Oxford, for a fellowship.

Registry No. $MoCp_2H_2$, 1291-40-3; WCp_2H_2, 1271-33-6; $W(MeCp)_2H_2$, 61112-90-1; $W(MeCp)_2Cl_2$, 63374-11-8; $W(MeCp)_2(C_2H_4)$, 87433-04-3; $W(MeCp)_2$, 87433-05-4; $EtAlCl_2$, 563-43-9.

Contribution from the Cancer Research Campaign Biomolecular Structure Research Group, Department of Biophysics, King's College, London WC2B 5RL, England, and Department of Chemistry, Birkbeck College, London WC1E 7HX, England

Crystal and Molecular Structure of Three Isomers of Dichlorodiamminedihydroxoplatinum(IV): Cis–Trans Isomerization on Recrystallization from Water

REIKO KURODA,*† STEPHEN NEIDLE,† ISMAIL M. ISMAIL,‡ and PETER J. SADLER*‡

Received July 27, 1982

The structures of the cis,cis,trans (compound I), trans,trans,trans (compound II), and cis,trans,cis (compound III) isomers of $PtCl_2(NH_3)_2(OH)_2$ have been determined by X-ray diffraction. In addition, I has been characterized in solution by ^{15}N and ^{195}Pt NMR. All compounds have closely octahedral coordination geometry for Pt(IV), normal Pt–O, Pt–N, and Pt–Cl distances, and extensive H-bonding networks in the crystals. A curious isomerization of II to III was observed on recrystallization from water but not from H_2O_2 solutions. This facile conversion was confirmed by X-ray crystallography and infrared spectroscopy.

There is considerable interest in the antitumor activity of Pt(IV) diammine complexes.[1] In some animal test systems they show superior activity to their Pt(II) analogues; for example, the therapeutic index for *cis,cis,trans*-$PtCl_2(NH_3)_2(OH)_2$ against the ADJ/PC6 tumor in BALB/C mice (28.1) is much higher than that for *cis*-$PtCl_2(NH_3)_2$ (8.1).[2] The axial hydroxyl groups often confer additional solubility on the complex, but in vivo it is suspected that they may be removed by reduction of the Pt(IV) complex to Pt(II). There is currently little evidence for this, although we have shown that thiols such as cysteine readily reduce *cis,cis,trans*-$PtCl_2(i\text{-}PrNH_2)_2(OH)_2$ in tissue culture media.[3]

There is little structural data available on Pt(IV) diammine complexes, and therefore we have embarked upon a study of the structures of the hydrogen peroxide oxidized adducts of Pt(II) diammine antitumor complexes both in the solid state and in solution, using primarily a combination of X-ray crystallography and multinuclear NMR spectroscopy. Our initial aim was to compare *cis,cis,trans*- and *trans,trans,trans*-$PtCl_2(NH_3)_2(OH)_2$ (compounds I and II, respectively). It was during the recrystallization of the latter complex from water that we discovered an unexpectedly facile isomerization involving the chloride and hydroxo ligands to produce a third isomer *cis,trans,cis*-$PtCl_2(NH_3)_2(OH)_2$ (compound III). Pt(IV) complexes are usually considered to be kinetically inert in solution.

Additional interest in platinum hydroxo complexes has been stimulated by the work of Rosenberg and Lock.[4,5] When our work was almost complete, we learned that they had also studied the crystal structure and vibrational spectra of compound I, and we therefore report our work only briefly where there is overlap.

Experimental Section

Compounds I and II were prepared by published procedures[6] involving the oxidation of *cis*- and *trans*-$PtCl_2(NH_3)_2$ with H_2O_2.

Table I. Infrared Data (cm^{-1}) for Isomers of $PtCl_2(NH_3)_2(OH)_2$[a]

cis,cis,trans (I)	trans,trans,trans (II)	cis,trans,cis (III)	assignt[b]
3510 (s)	3510 (s)	3460 (s)	ν(OH)
3255 (s)	3310 (s)	3290 (m)	
2950 (br, m)	3060 (s, br)	3200 }	
	2960 (s, br)	3120 }(m, br)	$\nu(NH_3)$
		3040 }	
2600 (s)	2680 (m)		
		2560 (m)	
2425 (m)		2420 (w)	
2240 (m)	2270 (w)	2290 (w, br)	
2180 (m)	1950 (w, br)		
	1770 (w, br)		
1590 (w)	1620 (m)	1615 (m)	$\delta(NH_3)$
1560 (w, br)	1600 (m)	1580 (m, br)	
	1560 (m)		
1415 (w)	1355 (m)	1345 (m)	
1300 (w)			
1270 (w)		1255 (m)	
1165 (m)	1170 (s)		
1105 (w)			
1040 (m)	960 (w)	1075 (m)	δ(PtO–H)
	905 (w)		
765 (m)		800 (w)	
690 (w)			
	568 (s)	580 (s)	}
540 (s)	530 (m, sh)	535 (m, sh)	} ν(PtO), ν(PtN)
505 (sh, m)	505 (m, br)	505 (m)	}
445 (m, br)			
330 (s)	350 (m)	335 (s)	} ν(PtCl)
	325 (m)		
275 (m)	290 (m, sh)		
	272 (m)		

[a] s = strong; m = medium; w = weak; sh = shoulder; br = broad. [b] See ref 5.

Anal. Calcd: H, 2.39; N, 8.39; Cl, 21.25. Found (I): H, 2.36; N, 8.39; Cl, 21.14. Found (II): H, 2.20; N, 8.43; Cl, 21.37. Found

(1) Tobe, M. L.; Khokhar, A. R. *J. Clin. Hematol. Oncol.* **1977**, *7*, 114.
(2) Cleare, M. J.; Hydes, P. C.; Hepburn, D. R.; Malerbi, B. W. In "Cisplatin, Current Status and New Developments"; Prestayko, A. W.; Crooke, S. T., Carter, S. K., Eds.; Academic Press: New York, 1980.

† King's College.
‡ Birkbeck College.

0020-1669/83/1322-3620$01.50/0